Applied Physics A (2018) 124:590
https://doi.org/10.1007/s00339-018-2015-5

Applied Physics A
Materials Science & Processing

Retention of carbon monoxide onto magnetic [BN fullerene: B_6]$^-$ and [BN fullerene: C_6]$^-$ nanocomposites

E. Chigo Anota[1] · M. Salazar Villanueva[2] · A. Bautista Hernández[2] · W. Ibarra Hernández[2] · M. Castro[3]

Received: 22 May 2018 / Accepted: 4 August 2018 / Published online: 9 August 2018

Abstract
The adsorption of the carbon monoxide molecules onto the magnetic [BN fullerene:B_6]$^-$ and [BN fullerene:C_6]$^-$ nanocomposites is analyzed by means of the density functional theory. Three nanostructures were considered to evaluate the interactions generated when molecules of CO are added until reach the saturation: magnetic pristine BN fullerene, BN fullerene functionalized with magnetic B_6 and C_6 clusters. For all cases, it is obtained a chemical interaction that was increasing with the number of CO molecules adsorbed. The above pristine [BNF:B_6]$^-$ and [BNF:C_6]$^-$ nanocomposites exhibit electronic behavior like-semiconductor; intrinsic magnetism (1.0 and 3.0 μ_B), high polarity, and low-chemical reactivity respect to pristine BNF; these quantum descriptors they are modified slightly when the [BN]$^-$ fullerene, [BNF:B_6]$^-$ and [BNF:C_6]$^-$ nanocomposites are interacting with carbon monoxide molecule, moreover high chemisorption is obtained. Therefore, it is feasible to propose these nanocomposites as CO sensors.

1 Introduction

Nowadays, one of the problems related to environment is to achieve the retention or degradation of pollutant molecules such as carbon monoxide or carbon oxide II (CO) [1–3]. This is a kind of gas highly toxic and it is produced due to the combustion defective of substances as gasoline, kerosene, coal, oil, tobacco or wood, among others. On the other hand, different nanostructures have been proposed as sensor of carbon monoxide (theoretically and experimentally), such as carbon nanotubes [4, 5], dioxide titanium surfaces [6], metal surface [7, 8], silver doped gold cluster [9, 10], zeolites [11], graphene supported Pd nanoparticles [12], boron nitride nanotubes and nanosheets [13, 14], etc. However, the nanocomposites formed between fullerenes and clusters still not have been studied to be applied as gas sensor. Recently, it was reported two clusters with features very attractive such as the octahedral Boron (B_6^-) cluster [15] with intrinsic magnetism (3.0 μ_B), electronic behavior-like semiconductor, low chemical reactivity, zero polarity, work function of 1.76 eV and high cohesion energy; as well as the non-planar (C_6^-) carbon cluster [16] with intrinsic magnetism (3.0 μ_B), low chemical reactivity, very low polarity, work function of 0.85 eV and cohesion energy similar to B_6^- cluster above mentioned, furthermore, these three-dimensional clusters indicate adequate structural stability. On the other hand, the boron nitride fullerene (BNF^-) [17] is a well-known nanostructure that exhibits electronic behavior-like semiconductor and intrinsic magnetism. Thereby, according the above information, in this work it is proposed the interaction of this fullerene with both clusters (BNF–B_6^- and BNF–C_6^-), then the two new nanocomposites will be tested as sensor gas, in specific interacting with one and several molecules of oxide of carbon. This study is organized in the next way: In Sect. 2 the methodology used in this work is described, the adsorption of carbon monoxide onto bare BNF, BNF:B_6 and BNF:C_6 composites are discussed in Sects. 3.1 and 3.2, respectively. The effect of saturation for six and fourteen CO molecules onto the whole fullerenes considered in this work is detailed in Sect. 3.3.1 and 3.3.2, respectively, and some conclusions are drawn in Sect. 4.

Electronic supplementary material The online version of this article (https://doi.org/10.1007/s00339-018-2015-5) contains supplementary material, which is available to authorized users.

✉ E. Chigo Anota
ernesto.chigo@correo.buap.mx

[1] Benemérita Universidad Autónoma de Puebla, Facultad de Ingeniería Química, Ciudad Universitaria, San Manuel, Código Postal 72570 Puebla, Mexico

[2] Benemérita Universidad Autónoma de Puebla, Facultad de Ingeniería, Apdo. Postal J-39, 72570 Puebla, Pue., Mexico

[3] Universidad Nacional Autónoma de México-Departamento de Física y Química Teórica, DEPg-Facultad de Química, C.P. 04510 Mexico, DF, Mexico

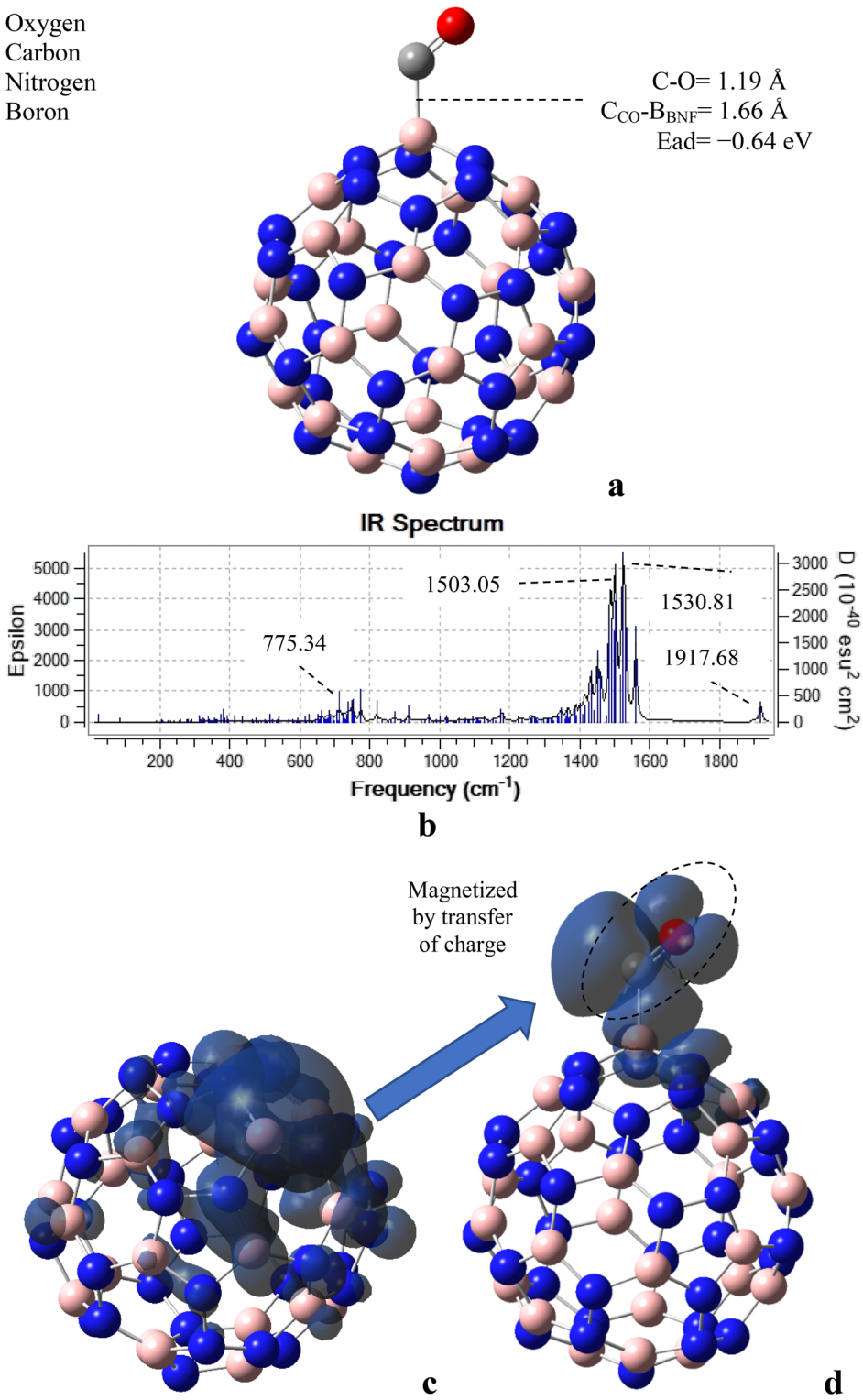

Fig. 1 **a** BNF–CO, **b** IR spectrum for BNF–CO and **c** total spin density surface for the BNF^{-}, and **d** the BNF–CO system for $Q=-1$ and $M=2$

2 Characteristics of simulations

First principles (spin-unrestricted) density functional theory or DFT [18] total energy calculations were done to study the interaction between a magnetic non-stoichiometric Boron Nitride fullerene (BNF^{-}; chemical composition $B_{24}N_{36}$) and Carbon monoxide (CO) molecule and magnetic $[BNF{:}B_6]^{-}$ and $[BNF{:}C_6]^{-}$ nanocomposites and CO molecule. In this case, it is analyzed when interacting with

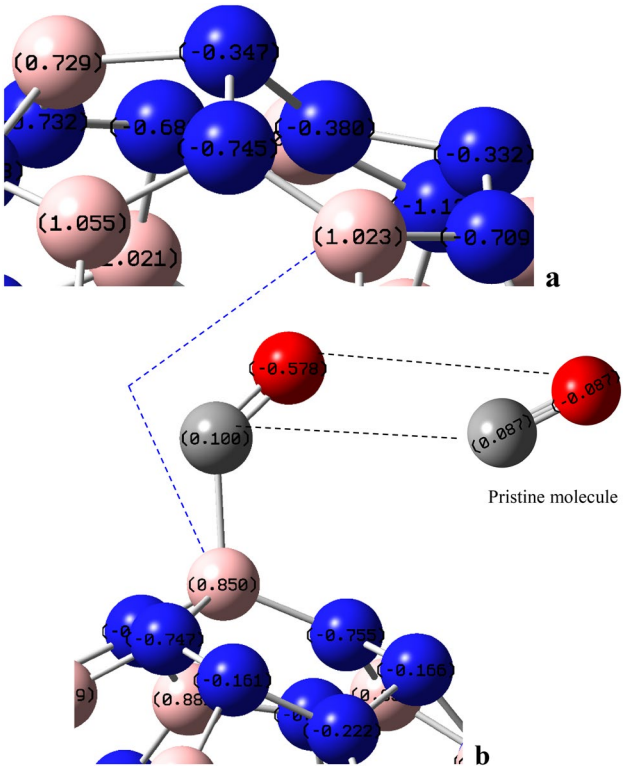

Fig. 2 NBO charges for **a** BNF, **b** BNF–CO (and CO molecule), **c** BNF:C_6, **d** pristine C_6^- cluster, **e** BNF:C_6–CO. Fragment showing the site of interaction

a molecule and when the nanocomposites are saturated. The B_6^- and C_6^- cluster used for the calculations presents non-planar geometry. In this work, anionic ($-1|e|$) system are analyzed for BNF$^-$–CO, [BNF:B_6]$^-$–CO and [BNF:C_6]$^-$–CO interactions. The results for [BNF:B_6]$^-$ and [BNF:C_6]$^-$ nanocomposites for the configuration of lowest energy were refined through the generalized gradient approximation (GGA) as proposed by Heyd, Scuseria, and Ernzerhof, (HSEh1PBE-GGA) [19], allowing for the description of large range interactions. Orbital 6-311g(d,p) basis set developed by Pople et al., were employed [20]. All-electron HSEh1PBE/6-311g(d,p) calculations were done with the quantum chemistry software GAUSSIAN-09 [21]. Tight convergence criteria were required in the stage of the geometry optimization. Employing an ultrafine grid, strict convergence was required for the total energy, minimized to 10^{-8} a. u. The geometries were optimized with a 10^{-4} a. u. threshold and for the RMS forces a 10^{-6} a.u. threshold was employed. To ensure the stability of the ground state vibrational calculations within the harmonic approximation, were carried out for the lowest energy structures without imaginary frequencies.

Seven, six and six geometric configurations were considered to analyze the interaction between BNF, [BNF:B_6]$^-$ and [BNF:C_6]$^-$ and CO molecule, see Table S1—Complementary material. The ground state for these configurations: BNF–B_6 [22], BNF–C_6, BNF–CO, BNF:B_6–CO and BNF:C_6–CO was found with the next parameters: anionic charge ($Q=-1$) and multiplicity ($M=2S_T+1=2$, 4, 2, 2, and 2; S_T = spin total). To avoid states of energetic degeneracy, the differences (E) between the multiplicities close to the most energetic are: 2.51, 2.88, 2.14, 1.24, and 0.66 eV, the energy proximity was solved for $M=4$,6, 4, 4 and 4.

Characterization of these systems was addressed by means of the global quantum descriptors [23]. The energy difference of the frontier LUMO and HOMO orbitals gives the average gap of the system; LHgap spin up $=(\varepsilon_{LUMO\uparrow}-\varepsilon_{HOMO\uparrow})/2\approx\varepsilon_{LUMO\uparrow}-\varepsilon_{HOMO\uparrow}$ and LHgap spin down $=(\varepsilon_{LUMO\downarrow}-\varepsilon_{HOMO\downarrow})/2\approx\varepsilon_{LUMO\downarrow}-\varepsilon_{HOMO\downarrow}$. The adsorption energy of carbon monoxide on the BNF surface and that of carbon monoxide on the [BNF:B_6]$^-$ and [BNF:C_6]$^-$ composites are defined as follows: $E_{ad}=E$[BNF–CO] $-E$[BNF] $-E$[CO] and $E_{ad}=E$[BNF:B_6–CO or BNF:C_6–CO] $-E$[BNF:B_6 or BNF:C_6] $-E$[CO]. The chemical potential (μ) or Mulliken electronegativity, being a measure of the average chemical reactivity, was approximated by the arithmetic average: $\propto=[(\varepsilon_{HOMO\uparrow}+\varepsilon_{HOMO\downarrow})/2+(\varepsilon_{LUMO}\uparrow+\varepsilon_{LUMO\downarrow})/2]/2$ [24], which for a free electron gas is equal to the Fermi level and is considered as the center of the energy gap. Besides, the average work function (WF) was estimated as the difference of the potential energy of the empty LUMO level and the Fermi energy (or chemical potential) and represents the minimal energy needed to remove an electron from the Fermi level into an empty level. This WF is a fundamental parameter in the design and control of electronic devices as it reported in the literature [25, 26].

3 Results and discussion

3.1 Adsorption of carbon monoxide on magnetic [BNF]$^-$

Seven geometric configurations were considered to obtain the lowest energy structure to the pristine BN fullerene and a carbon monoxide (CO) molecule, this search was focused on the hexagon formed by 1B5N, see Table S1—Complementary material. The configuration 3 (Fig. 1a) is the most stable in energy, with $Q=-1$ and $M=2$ such as it is indicated in complementary materials. Here, the CO molecule suffers a stretched in the bond length up to 1.19 Å compared to the isolated case (1.13 Å). The carbon atom is bonded to boron atom of fullerene, the bond length generated is 1.66 Å. These values lead to chemisorption effect (−0.64 eV), in a good agreement with the previously reported such as on some sites very particular for non-stoichiometric BN fullerene [27] ($E_{ad}=-0.27$

Table 1 Bond length (Å), HOMO–LUMO gap (LHgap; eV), dipolar moment (Debye), average chemical potential (μ; eV), average work function (eV), moment magnetic (μ_B), adsorption energy (eV) for BNF, BNF:B_6, BNF:C_6, BNF:B_6–CO and BNF:C_6–CO systems

Systems	Bond length	LHgap	Dipolar Moment	μ	Work function	Magnetic moment	Adsorption energy
$[BNF]^-$ [17]	1.42,1.43 (B–N) 1.42–1.46 (N–N)	0.80↑ 2.42↓	8.19	−4.87	0.80	1.0	
$[BNF:B_6]^{-a}$ [22]	1.42,1.43 (B–N) 1.42–1.46 (N–N) 1.58–1.92 (B–B)	1.38↑ 0.10↓	20.84	−5.94	0.37	1.0	−8.52
$[BNF:C_6]^{-a}$	1.42,1.43 (B–N) 1.37–1.59 (C–C) 1.44[b] (C–N)	2.62↑ 0.30↓	19.42	−6.22	0.73	3.0	−2.85
BNF–CO[a]	1.42,1.43 (B–N) 1.66[b] (B–C)	1.13↑ 1.33↓	11.58	−4.97	0.62	1.0	−0.64
$[BNF:B_6]$–CO[a]	1.42,1.43 (B–N) 1.42–1.46 (N–N) 1.56–1.82 (B–B)	1.80↑ 0.04↓	19.08	−6.45	0.46	1.0	−1.91
$[BNF:C_6]$–CO[a]	1.42,1.43 (B–N) 1.29[b] (C–C)	1.15↑ 0.15↓	11.46	−6.64	0.33	1.0	−1.33

[a]Minimal energy structure

[b]Minimum interaction distance

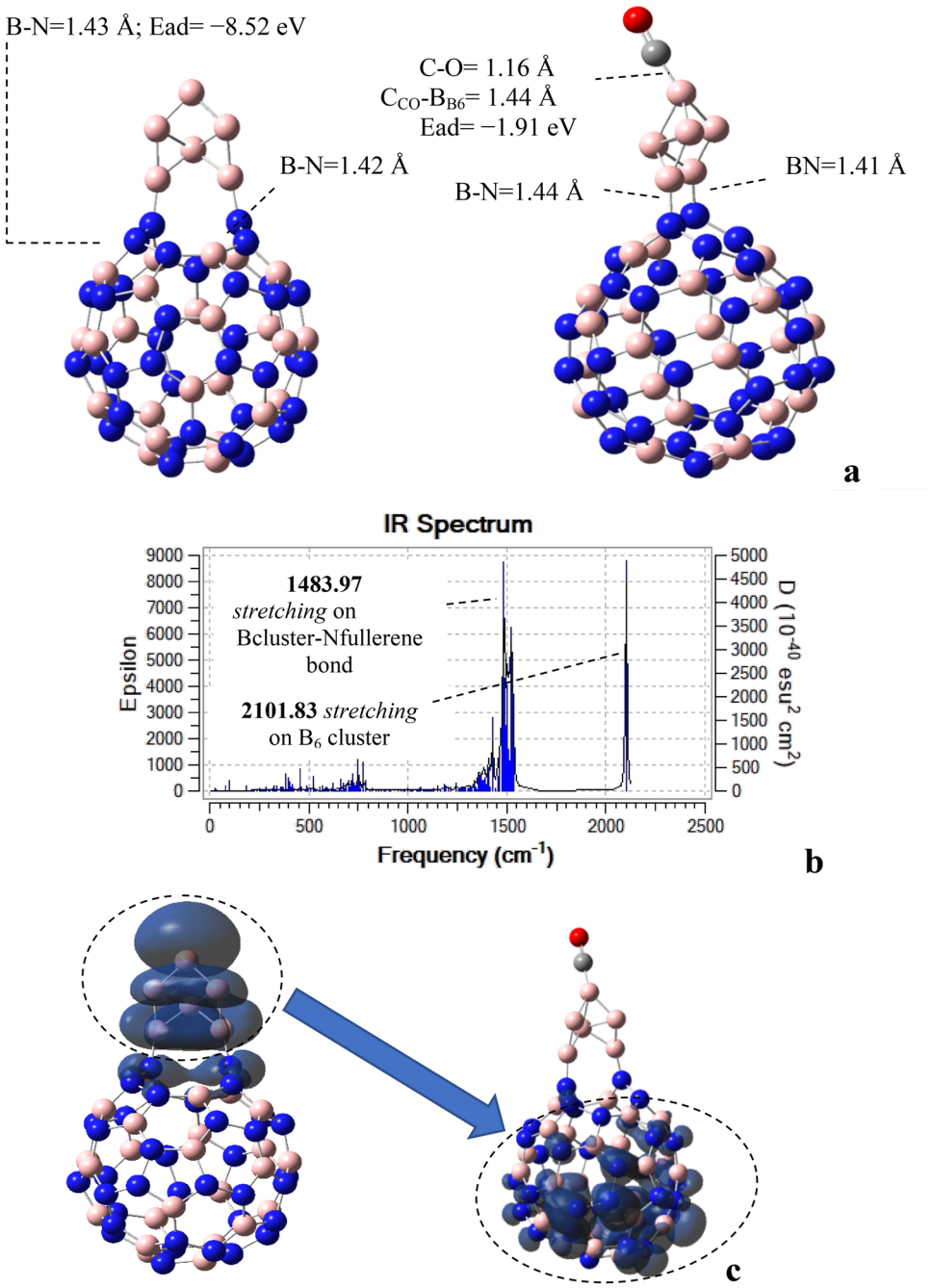

Fig. 3 **a** [BNF:B_6]$^-$ and [BNF:B_6]$^-$–CO system for $Q=-1$, $M=2$, **b** IR spectrum for [BNF:B_6]$^-$–CO system and **c** total spin density surface for BNF:B_6 and [BNF:B_6]$^-$–CO system

to −1.78 eV) and when an electrical field is applied on hexagonal BN nanosheet [28] to improve the adsorption (−0.84 eV). As comparative data, in the systems based on Al-doped and N-doped graphene the adsorption values reported are also within the range of chemisorption (−0.5 eV) and physisorption (−0.03 eV), respectively [29, 30].

This positive adsorption is due to the electronic transference from fullerene toward CO molecule ($\Delta Q=0.17$ |e|) according to Natural Bond Orbital (NBO) [31] analysis, this effect is illustrated in Fig. 2a, b, respectively. Moreover, this charge transference lead to high polarity (11.58 *D*), however, the semiconductor behavior remains despite of CO molecule is bonded to fullerene (average LHgap = 1.23 eV), here the contribution of spin up and down is similar, see Table 1. This BNF–CO system shows a low average chemical reactivity and average work function (0.62 eV), which indicates the covalent functionalization of this fullerene by means organic molecules and this effect can help us to design new devices. The moment magnetic is not alternated with respect pristine case (1.0 μ_B), however, according to spin density isosurfaces (Fig. 1c, d), the magnetism flows from fullerene toward CO molecule by means of intermolecular plus intramolecular

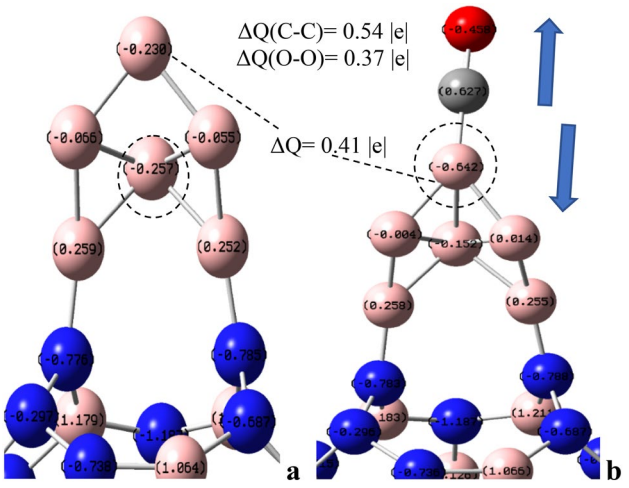

Fig. 4 NBO charges for **a** BNF:B_6 and **b** BNF:B_6–CO. The difference in charge is made with respect to the pristine CO molecule

mechanisms, in agreement to electronic transference above mentioned.

The calculation of infrared (IR) spectrum for this system was obtained to ensure the vibrational stability, no imaginary modes were obtained (see Fig. 1b). This spectrum indicates peaks related to stretching movement out of plane at 775.34 cm^{-1}, and at 1503.05 and 1530.81 cm^{-1} oscillations associated to B–N bonds in agreement to BN spheres recently reported [32, 33]. Moreover, there is shorting in the value of stretching mode of CO molecule from 2246.52 cm^{-1} (isolated molecule) up to 1917.68 cm^{-1}, this effect indicates strong bonding between CO complex and pristine fullerene.

3.2 Adsorption of carbon monoxide on the $[BNF:B_6]^-$ and $[BNF:C_6]^-$ composites

The covalent functionalization of the BNF with B_6 [15] and C_6 [16] clusters have been previously reported and their properties are summarized in Table 1 as well as for the first case is illustrated in Figs. 2a, 3a–c and 4a; and the latter case in Fig. 5a–c, respectively.

Then, first the $[BNF:B_6]^-$ nanocomposite is bonded to a CO molecule, and six possible configurations were considered for this interaction; which the number 3 was the most stable, here the CO molecule in the perpendicular way to one carbon and boron atom of nano-composite. This effect generates a length bond of 1.44 Å between them and an adsorption energy associated of − 1.91 eV, besides the boron (B_6) cluster remains with its pyramidal structure as well. The bond length of CO molecule chemisorbed on BNF:B_6 is stretch up to 1.16 Å respect to isolated molecule (1.13 Å) but this value is minor with respect to CO−BNF system (1.19 Å), this short bond lead for BNF:B_6 cluster stronger adsorption than pristine case (BNF). The above statements can be explained by means the electronic transference due to the carbon atom shares charge to oxygen and boron atom on adsorption site, with the next charge differences: $\Delta Q(C) = 0.54$ $|e|$, $\Delta Q(O) = 0.37$ $|e|$ and $\Delta Q(B) = 0.4$ $|e|$, respectively (see Fig. 4a, b) and in this way the electronic transference plays a crucial role on the adsorption effect. It must be mentioned the fact that the boron atom is marked on dashed circle in Fig. 4a, this gives part of its charge to the opposite boron atom (Fig. 4b). Furthermore, the strong interaction between BNF:B_6 and CO molecule is due to this high electronic transference on the adsorption site. The latter effect generates an electronic value of 0.92 eV for average LHgap (with a greater contribution of the spin up), which is similar in behaviour to the BNF:B_6 system (average 0.74 and 1.61 eV for BNF) as well as the average chemical reactivity and work function are not affected, however, its polarity suffers a great increase, around a factor of 5.02 respect to pristine BNF case (see Table 1). According to total spin density isosurfaces, the magnetism is displayed at bottom of the fullerene on the boron and nitrogen atoms (see Fig. 3c), apparently due to the electronic charge is concentered on the adsorption site and, furthermore, on the rest of fullerene there are unpaired electrons that generate magnetism useful for different applications. The values obtained from IR spectrum (Fig. 3b) show just real values without imaginary ones, there, one peak at 1483.97 cm^{-1} associated to stretching movement on the surface fullerene is observed and other similar movement is localized at 2101.83 cm^{-1} for the molecule of CO, and a new a shortening of this value respect to isolated molecule (2246.52 cm^{-1}) is obtained and this effect leads to positive adsorption too.

For the CO molecule on BNF:C_6 composite, the most stable structure of the six considered, the first one was obtained as the ground state (see Fig. 6a). This chemical interaction generates a bond length between them of 1.29 Å and a chemisorption energy of − 1.33 eV as well as the bond length of CO suffers a slightly stretch up to 1.17 Å besides the carbon cluster presents some changes in its bonds from 1.38 up to 1.56 Å on C–C lengths.

These structural modifications are results of the adsorption of CO molecule on BNF:C_6, the electronic transference is responsible of latter effects, thus there is a decreasing transference of charge for carbon atom and boron atom on adsorption site between carbon cluster and fullerene (see Fig. 7b, d) and the carbon atom of CO molecule address its charge toward oxygen atom and carbon atom of the cluster. Thereby, the CO molecule is thigh bonded on carbon cluster, however, the adsorption of the CO−C_6 composite on BNF is weaker than the BNF:B_6−CO cluster, in agreement with data of Table 1. The charge transfer generates a reduction in the gap conserving its semiconductor behavior for the BNF:C_6−CO composite (average LHgap = 0.65 eV; in the

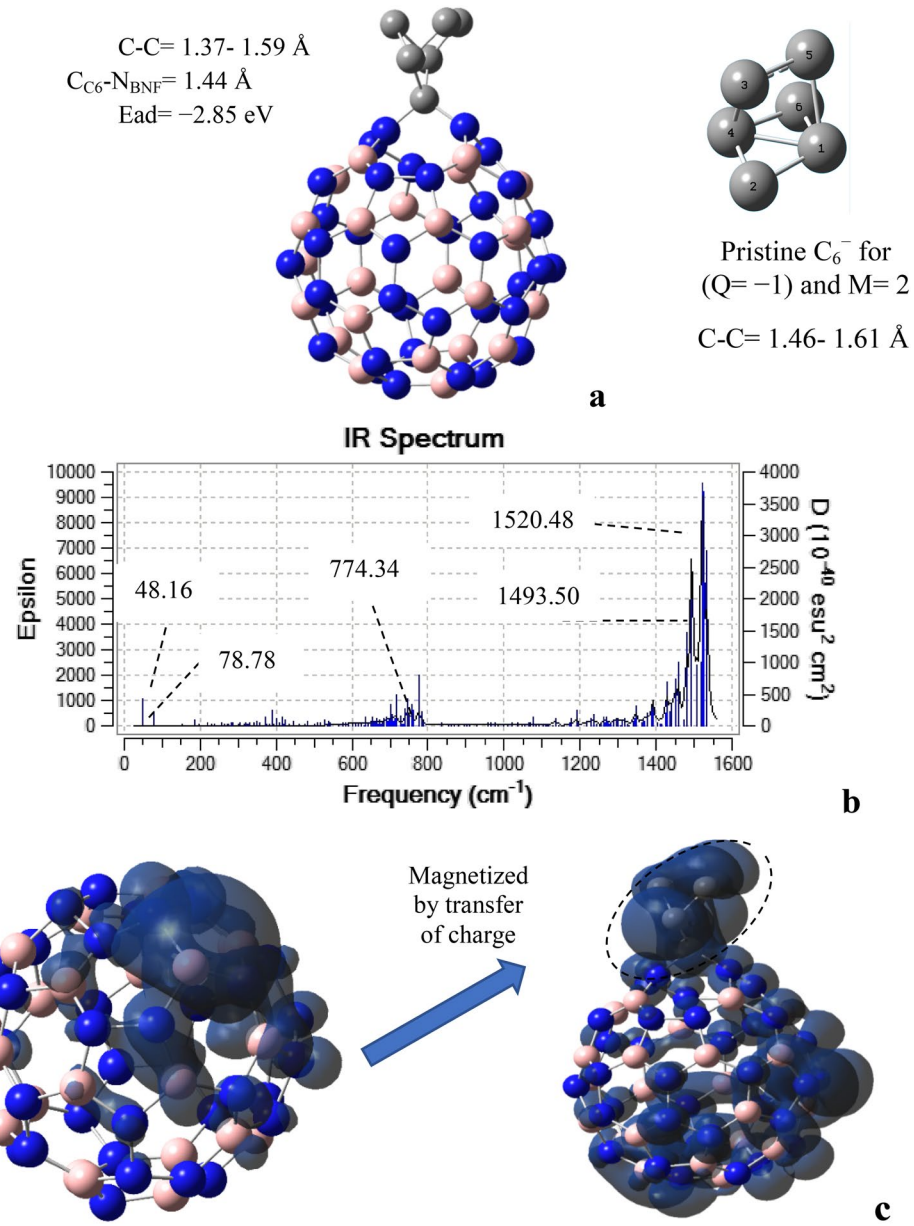

Fig. 5 **a** [BNF:C_6]$^-$ structure for $Q=-1$, $M=4$, **b** IR spectrum, and **c** total spin density surface for BNF and BNF:C_6

same way the biggest contribution comes from the spin up with 1.15 eV), as well as the polarity is reduced compared to pristine BNF:C_6 case (11.46 *D*). However, the average chemical reactivity is not affected and the parameters that suffer reduction are average work function (0.33 eV with respect to the BNF:C_6 that presents a value of 0.73 eV) and the magnetic moment (1.0 μ_B), this last due to the spin density is displayed on the BN fullerene (see Fig. 6c), since the electronic transference is localized on the adsorption site and this effect generates paired electrons on the fullerene surface. On the other hand, the spectrum (Fig. 6b) reveals just real values, furthermore the vibrational stability is ensured. There is a stretching movement associated to the surface of BNF at 391.78 and 1483.55 cm^{-1}, one wagging at 547.30 cm^{-1} generated by the interaction between carbon cluster and CO molecule. There is a characteristic peak at 2259.05 cm^{-1} related to CO stretching movement, this value is larger than the isolated CO molecule, however, this effect leads to positive adsorption.

3.3 Effect of saturation of CO molecules on pristine and nanocomposites fullerenes

To understand the adsorption of CO molecules on the pristine and composites fullerenes under experimental conditions, in this study (CO)*n* molecules distributed in a random way onto them have been considered to simulate the effect of saturation on latter systems, with $n=6$ and 14 molecules to

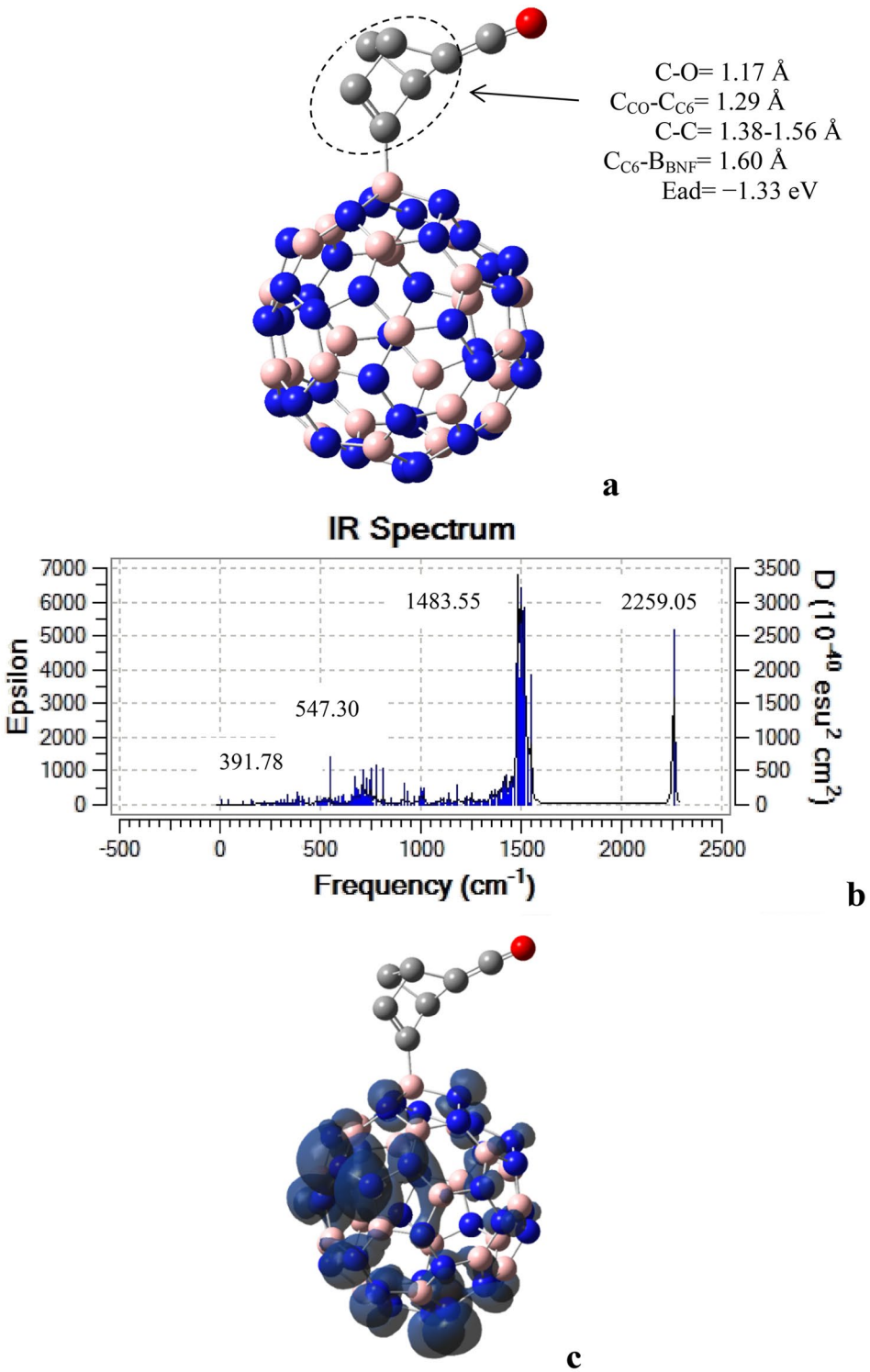

Fig. 6 **a** BNF:C_6–CO for $Q=-1$, $M=2$, **b** IR spectrum, **c** total spin density surface where magnetism is concentrated on fullerene

establish a tendency on adsorption and thus evaluate the possible application as sensor or storage of monoxide of carbon. There are two possible paths: (i) attach the CO molecules by the cluster side or (ii) by pristine zone; the first option was performed due to this geometric configuration is the most chemically active.

3.3.1 Saturation with $(CO)_6$

The BNF−CO_6 system is not stable according to vibrational calculation with some imaginary modes, furthermore, this is discarded for discussion. The ground state for BNF:B_6–$(CO)_6$ system was found with anionic charge and

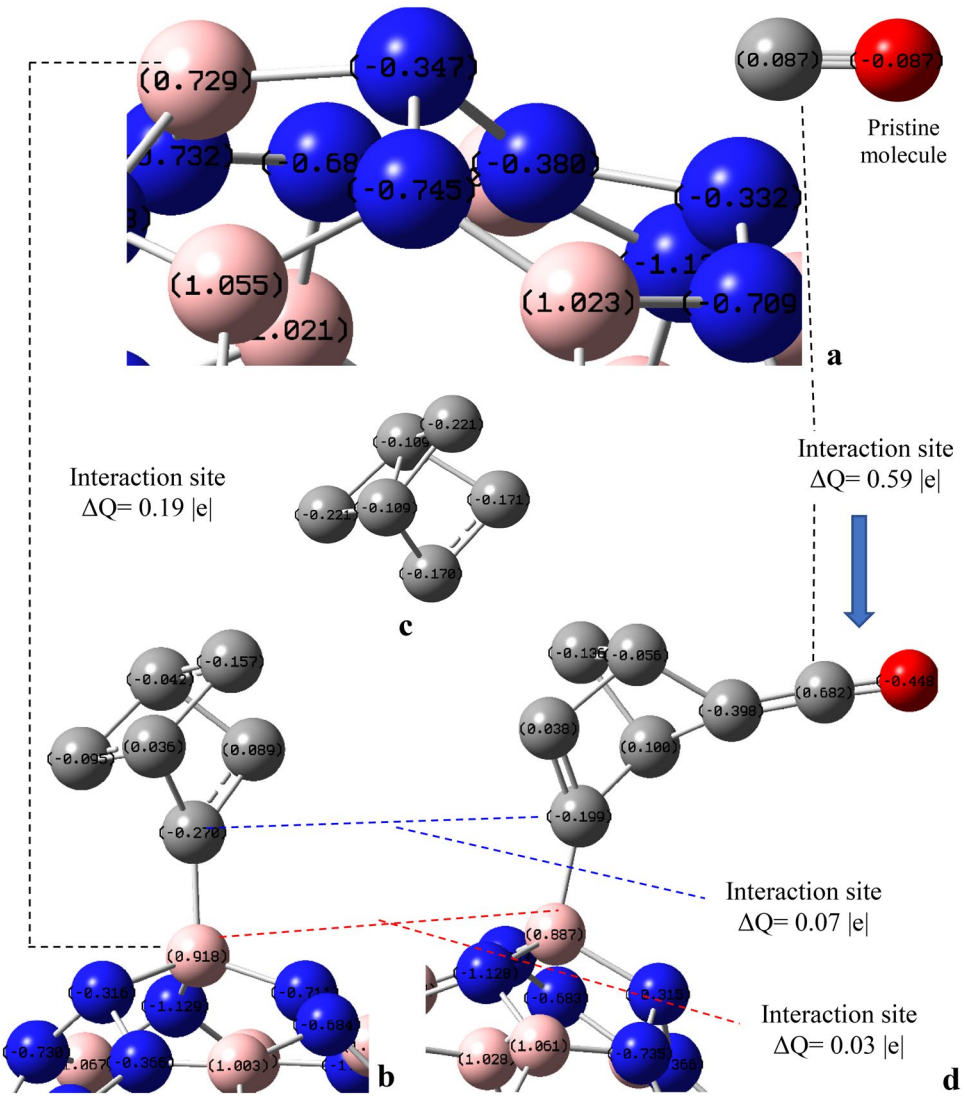

Fig. 7 NBO charges for **a** BNF, **b** BNF:C_6, **c** pristine C_6^- cluster, **d** BNF:C_6–CO. Fragment showing the site of interaction

multiplicity 2 as it is observed in Fig. 9a and its stability was ensured by means vibrational calculation, where just real values are obtained (see Fig. 9b). The value of adsorption energy is increased from − 1.91 up to − 7.19 eV, the above for one and six CO molecules, respectively; therefore, the binding is more favored almost 3.7 times for larger number of CO molecules than just with one molecule. This effect can be explained by means the MEP of BNF:B_6–$(CO)_6$ (Fig. 10a) system that shows the electronic transference happens from BNF plus boron cluster toward CO molecules, moreover, the charge is localized on the oxygen atoms of carbon monoxide molecules bonded to boron cluster.

This high chemical interaction generates structural change on B_6^- cluster, since this is transformed in a regular pentagonal pyramid with values of B–B bonds from 1.66 up to 1.83 Å, as well as the length bonds between cluster and BN fullerene are stretched up 1.45 and 1.48 Å, compared to BNF:B_6 case (1.42 and 1.43 Å).

On the other hand, the quantum parameters as average chemical reactivity, polarity remains almost invariant, average LHgap = 0.70 eV, here the major contribution of the spin down gives 0.76 eV and average work function remains with negligible changes, see Table 2. However, one drastic change was observed on the spin density of BNF:B_6–$(CO)_6$ system, due to this isosurface is displayed on the CO molecules bonded to B_6 cluster, in specific on the B–O–C bond (see Fig. 9a), this is opposite to the case of just one molecule attached, this is displayed on the fullerene surface (see Fig. 3c). Despite of this fact, the value of magnetic moment remains in 1.0 μ_B.

On the other hand, for BNF:C_6–$(CO)_6$ nanocomposite (see Fig. 11a) the ground state was found under the next parameters as latter case: $Q = -1$ and $M = 2$. The adsorption energy of this system (− 3.68 eV) is 2.76 times larger

Table 2 Bond length (Å), LUMO–HOMO gap (LHgap; eV), Dipolar moment (Debye), Average chemical potential (μ; eV), Average work function (eV), Moment magnetic (μ_B), Adsorption energy (eV) for BNF, BNF:B_6, BNF:C_6, BNF:B_6–CO and BNF:C_6–CO systems

Systems	Bond length	LHgap	Dipolar Moment	μ	Work Function	Magnetic Moment	Adsorption energy
BNF–$(CO)_{14}$[a]	1.42,1.43 (B–N)	0.98↑ 1.16↓	11.18	−5.66	0.54	2.0	−1.15
[BNF:B_6]–$(CO)_6$[a]	1.42,1.43 (B–N) 1.42–1.46 (N–N) 1.66–1.83 (B–B)	0.63↑ 0.71↓	14.45	−6.21	0.35	1.0	−7.19
[BNF:B_6]–$(CO)_{14}$[a]	1.42,1.43 (B–N) 1.42–1.46 (N–N) 1.74–1.85 (B–B)	0.80↑ 0.10↓	16.40	−6.19	0.23	1.0	−8.58
[BNF:C_6]–$(CO)_6$[a]	1.42,1.43 (B–N) 1.40–1.61 (C–C)	1.12↑ 0.23↓	16.88	−6.68	0.34	1.0	−3.68
[BNF:C_6]–$(CO)_{14}$[a]	1.42,1.43 (B–N) 1.402–1.56 (C–C) 1.53 (C–N) 1.58 (C–B)	1.76↓ 0.35↓	11.24	−6.46	0.49	2.0	−4.86

[a]Minimal energy structure

than BNF:C_6–CO nanocomposite, this effect is associated to one geometric reconfiguration of C_6 cluster such as boron case (see Fig. 5a) from three-dimensional configuration to irregular pentagonal pyramid (see Fig. 11a), however, the values of bonds length remains almost without alteration (1.40–1.61 Å) respect to pristine case (1.46–1.61 Å). The adsorption is improved in better way for boron case than carbon case, due to the C_6 cluster and BN fullerene are forming just one bond with 1.57 Å of distance; and for the case of BNF:C_6–CO this value is 1.60 Å, this narrowing on length bond advantages in adsorption to BNF:C_6–$(CO)_6$ nanocomposite.

This effect is explained by means the MEP of BNF:C_6–$(CO)_6$ system (Fig. 10b) that shows the electronic transference happens in similar way that above nanocomposite, from BNF plus carbon cluster toward CO molecules that are bonded to BNF:C_6 system, however, three carbon monoxide molecules are not bonded straightforward manner to carbon cluster and thereby the adsorption energy of this nanocomposite is lesser than the previous one that consider boron cluster. The stability of this system was ensured by means of vibrational calculation, where no imaginary modes (Fig. 11b) were obtained. All their quantum descriptors do not change in a drastic way with respect pristine case as well as the isosurface of spin density (see Fig. 11b) and the value of the moment magnetic.

3.3.2 Saturation with $(CO)_{14}$

In summary, the following Figs. 8, 9, 10, 11, 12 and Table S2—Complementary materials indicate the results of the saturation. The ground state of BNF–$(CO)_{14}$ system (Fig. 8a) is obtained with the next parameters: $Q = -1$ and multiplicity = 4, after analyzing the multiplicity and obtaining the real vibrational modes, such as it was described in the previous cases.

According to the value of adsorption energy (− 1.15 eV), this complex is considered within chemisorption range; therefore, the CO molecules are bonded to BNF cluster in a strong way. However, it is observed that few molecules present bond with BNF and the other ones are around apparently without bond. The above interaction generates a semiconductor electronic behavior (average LHgap = 1.07 eV and with the highest contribution of the spin down of 1.16 eV), a low average chemical reactivity (− 5.66 eV) and a value of 0.54 eV for an average work function. These changes are due to the strong electronic transference form BNF toward CO molecules, however, the charge is concentered on the two CO molecules close to BNF and with minor intensity around of the rest ones, according MEP of this nanocomposite (Fig. 10c). Moreover, the isosurface of spin density (Fig. 8c) is localized on the stronger interaction site and over the neighbor molecules. The vibrational stability was

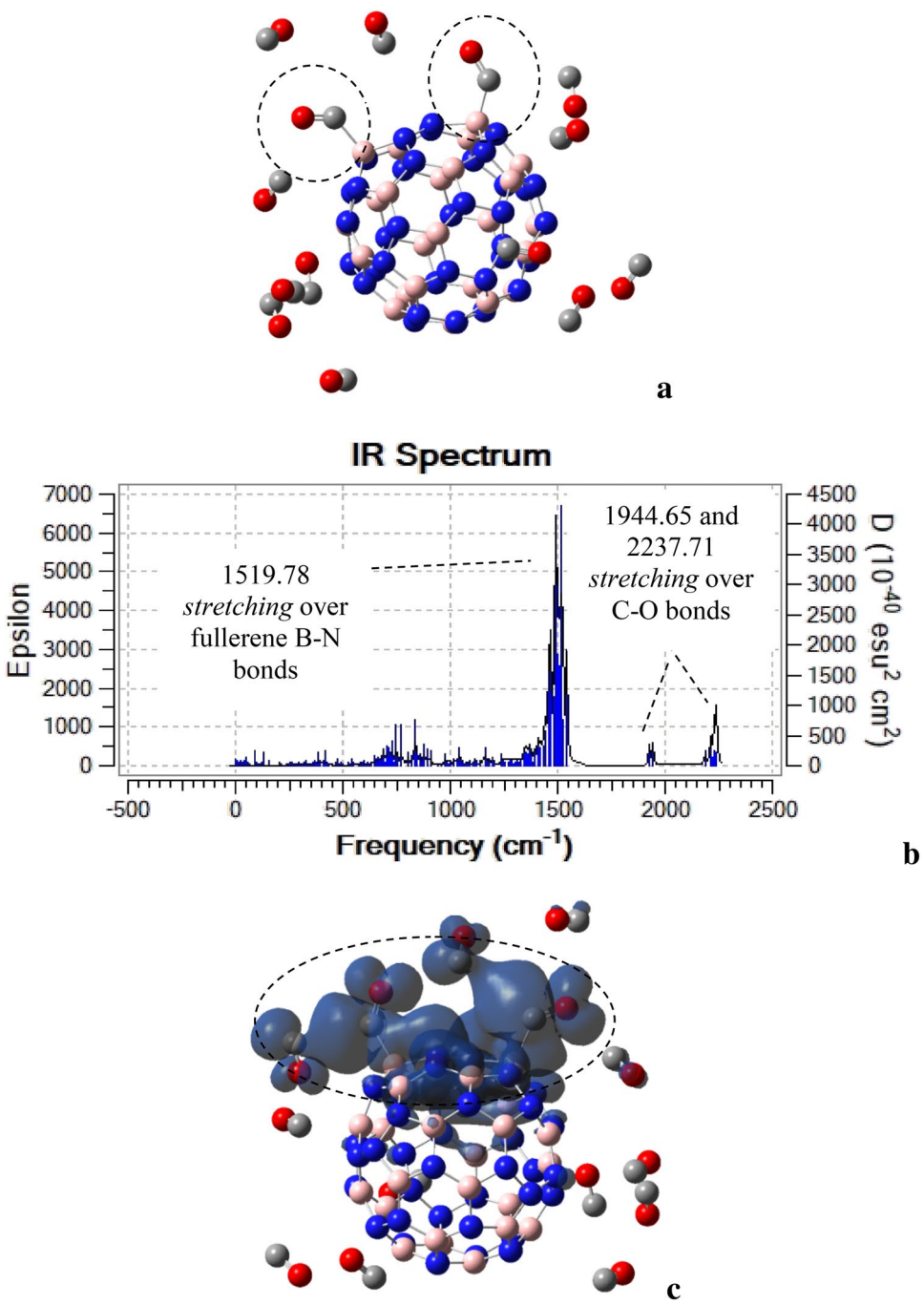

Fig. 8 **a** BNF–$(CO)_{14}$ molecules for $Q=-1$ and $M=4$, **b** IR spectrum and total spin density surface localized on BN fullerene and CO molecules

suggested by means calculation of IR spectra, without imaginary modes, see Fig. 8b.

Now, we are focusing on functionalized cases with the same quantity of CO molecules to be compared with the latter case. The first case, BNF:B_6–$(CO)_{14}$ system, see Fig. 12a its ground state is obtained with $Q=-1$ and multiplicity = 2, see Table S2—Complementary material. It is observed the formation of one pentagon between carbon and boron atoms, in specific by three CO three CO molecules and one boron atom of cluster localized in one vertex of pyramidal structure (P.S) such as it is indicated in Fig. 12a. This interaction generates the increases of B–B bond length for this P.S., from 1.74 up to1.85 Å due to the adsorption of CO molecules around of boron cluster, this distortion is most notable for 14 than 6 CO molecules for this nanocomposite. The average LHgap = 0.45 eV indicates an electronic behavior still within the range of semiconductors; here a great contribution of the spin up is observed from 0.80 eV, also a low average chemical reactivity (− 6.19 eV) as well as the average

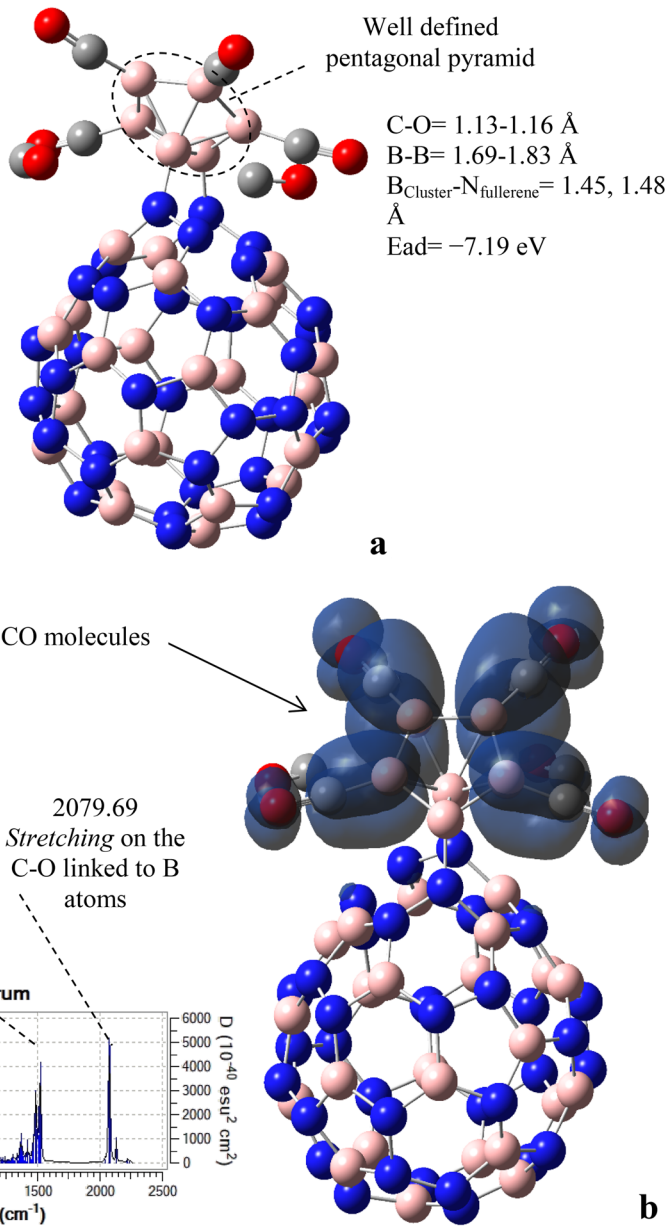

Fig. 9 **a** BNF:B_6–$(CO)_6$ molecules for $Q=-1$ and $M=2$, **b** IR spectrum and total spin density surface localized on BN fullerene

work function of 0.23 eV. A high polarity (16.40 *D*) is also observed as in previous cases.

The value of adsorption energy suffers an increase up to −8.58 eV (see Table 2), however this value is close to the correspond to the case of six CO molecules (−7.19 eV), which indicates that the saturation point of the number of CO molecules is almost reached at least for this system. These parameters lead to this nanocomposite as good sensor and nanomaterial for retention of this CO molecule. The rest of quantum descriptors remain in analogue way as BNF:B_6–$(CO)_6$ system. It must be mentioned the fact of the CO molecules are bonded just around the boron cluster, and this effect generates a tight and uniform electronic transference from BNF:B_6 nanocomposite toward CO molecules, as it can be appreciated in the correspond MEP (see Fig. 10d). This electronic redistribution generates the best adsorption of the whole systems studied in this work.

On the other hand, the magnetism of BNF:B_6–$(CO)_{14}$ system is displayed on the fullerene as it is appreciated in the isosurface of spin density (see Fig. 12c), besides the magnetic moment value is 1.0 μ_B. The adsorption of CO molecules lead to this important magnetic effect and the spin distribution is similar than the case of one CO molecule (see Fig. 3c) but different to case of six CO molecules (see Fig. 9b), respectively. Therefore, this magnetism induced help to remain bonded to the CO molecules with this nanocomposite. Here, the electronic transference plays a very important role again, although the charge migrates

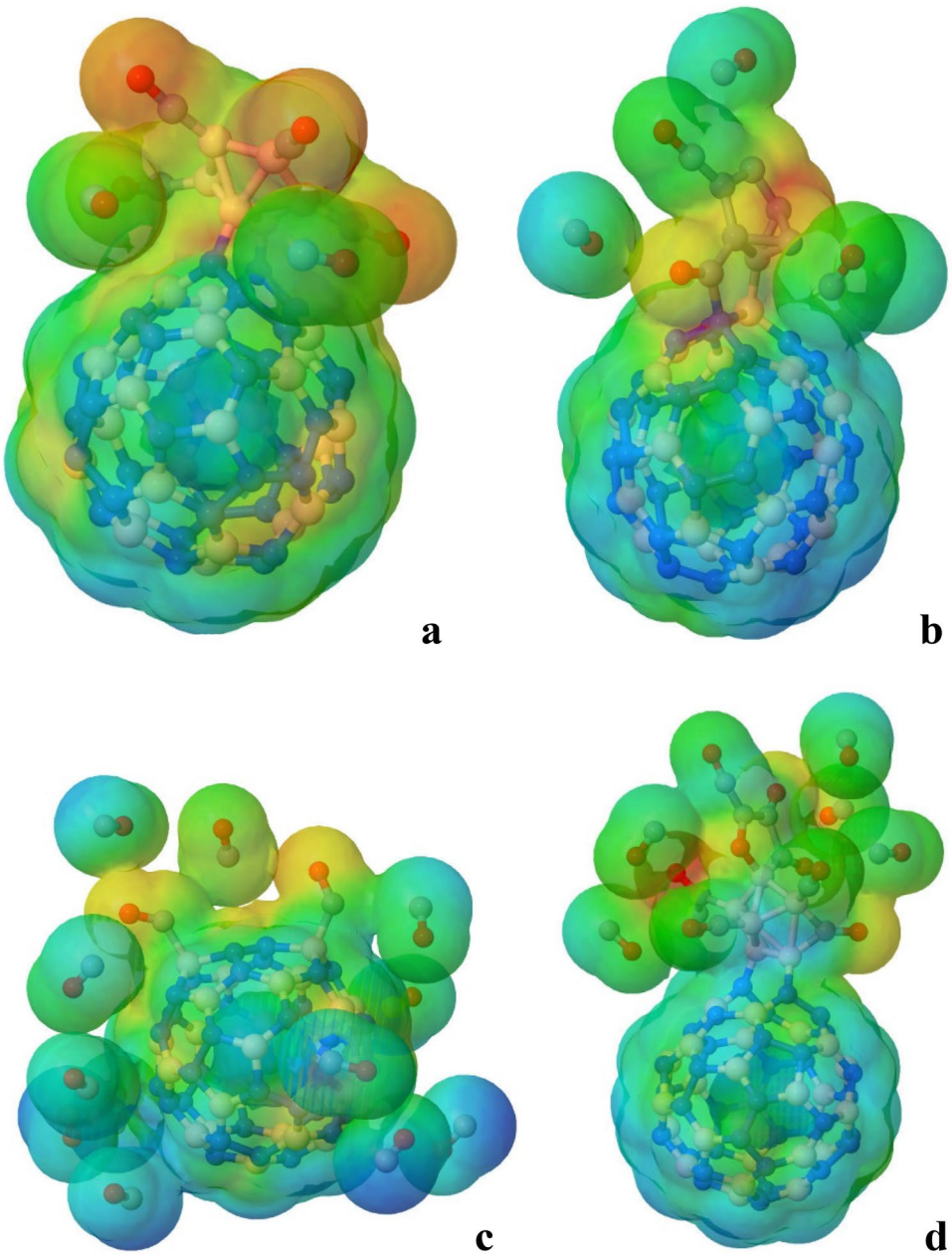

Fig. 10 MEP isosurface (*e*/bohr^3; red: negative) for **a** BNF:B_6–$(CO)_6$, **b** BNF:C_6–$(CO)_6$, **c** BNF–$(CO)_{14}$, **d** BNF:B_6–$(CO)_{14}$

from BNF:C_6 toward CO molecules as well, some molecules are bonded in a way strong and the rest around of them, however, this fact does not mean that there is weak adsorption, but this value is minor than boron case.

The stability was ensured by means of calculation of IR spectrum, Fig. 12b without imaginary modes. In the above figure are observed peaks at 1031.58 cm^{-1} that are associated to stretching movement generated by the oxygen atom (CO molecule) bonded to one boron atom of the cluster. The peaks at 1261.91, 1370.70, 1483.79 and 1510.28 cm^{-1} come of B–N bonds of fullerene as well as peaks at 2126.53 and 2241.51 cm^{-1} correspond to the contribution of C–C of CO molecules bonded and non-bonded, respectively (see Fig. 12a) and all of them with stretching movement too.

Now, we are going to addressing the discussion on BNF:C_6–$(CO)_{14}$ system, Fig. 13a. This exhibit the same parameters than ground state for one CO molecule: ($Q = -1$) and multiplicity = 4, see Table S2—Complementary material. The value of adsorption energy for this complex is −4.86 eV, furthermore a covalent interaction was obtained due to the CO molecules are bonded to the nanocomposite in a thigh way. On the interaction site two bond are formed between a CO molecule and fullerene, this length is around of 1.53 Å, hence the distances $C_{Cluster}$–N_{BNF} and $C_{Cluster}$–B_{BNF} are enhanced up to 1.58 Å, respect to pristine

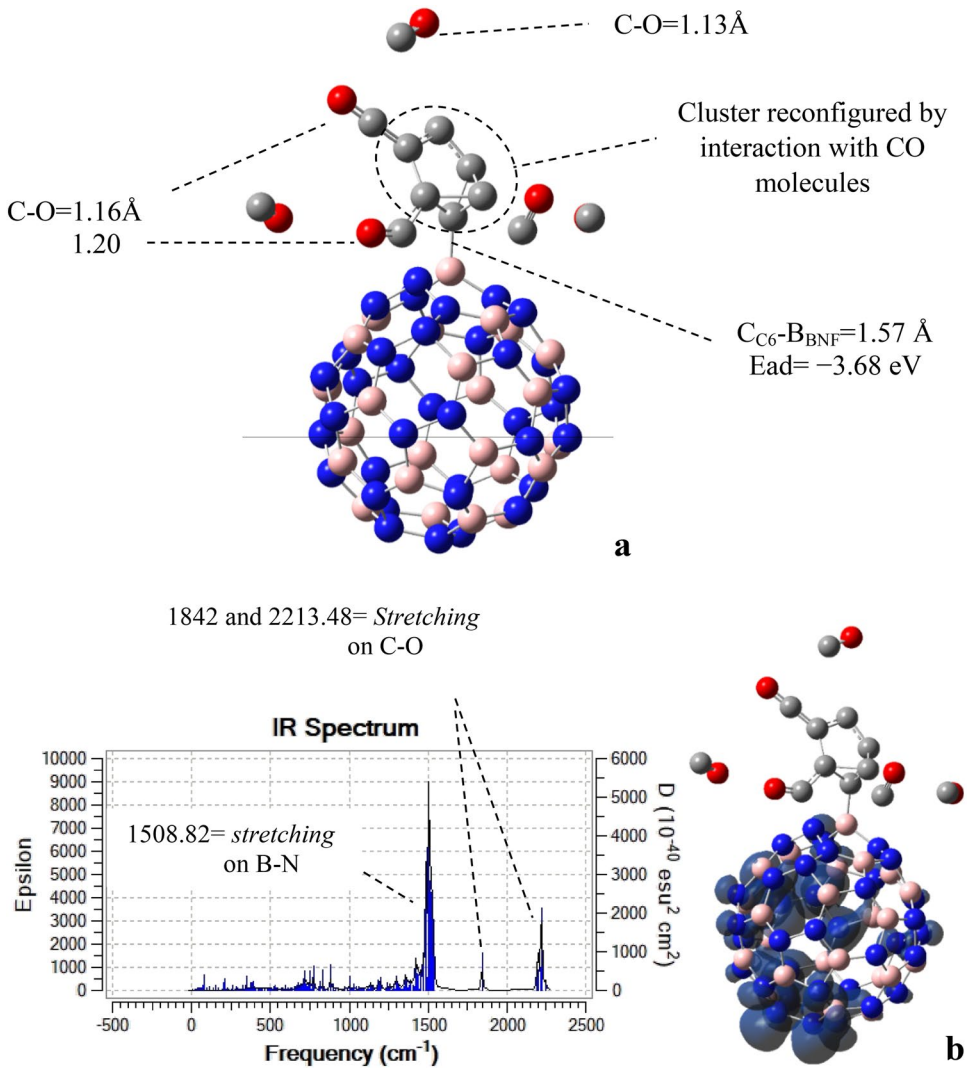

Fig. 11 **a** BNF:C_6–$(CO)_6$ molecules for $Q=-1$ and $M=2$, **b** IR spectrum and spin density surface localized on BN fullerene

nanocomposite. Moreover, on this surface it is observed a dissociation of B–N bond associated to BNF. The CO molecules non-bonded remain their values at 1.13 Å and those of bonded to the cluster oscillate in the range of de 1.16, 1.17, 1.22 and 1.30 Å, respectively.

On the other hand, the isosurface of spin for BNF:C_6–$(CO)_{14}$ system is displayed in homogenic way on: some CO molecules, C_6 cluster and the fullerene (Boron and nitrogen atoms) according Fig. 13c. The distribution of electronic charge due to CO molecules saturation generates this magnetism as well as the value is enhanced up to 2.0 μ_B. This statement is different when 1 (Fig. 6c) and 6 (Fig. 11b) molecules of CO are adsorbed.

In this case of saturation, the average LHgap = 0.96 eV indicates an electronic behavior still within the range of semiconductors; here a great contribution of the spin up is observed from 1.76 eV, also a low average chemical reactivity (− 6.46 eV) as well as the average work function of 0.46 eV. A high polarity (11.24 *D*) is also observed for this case.

The vibrational stability was ensured as in the above cases, by means IR spectrum, (Fig. 13b) calculation without imaginary modes. Once time, the stretching movements government the vibrations on this nanocomposite, i.e., the most characteristics are localized at 1499.89 and 1769.74 cm^{-1}; these are generated by the interaction of the bond formed between BN fullerene and C–C cluster, as well as two molecules of CO bonded between them and with the BNF. At 2165.16 and 2203.85 cm^{-1} appear peaks associated to CO molecule adsorbed onto another CO molecule and both bonded to C_6 cluster, respectively.

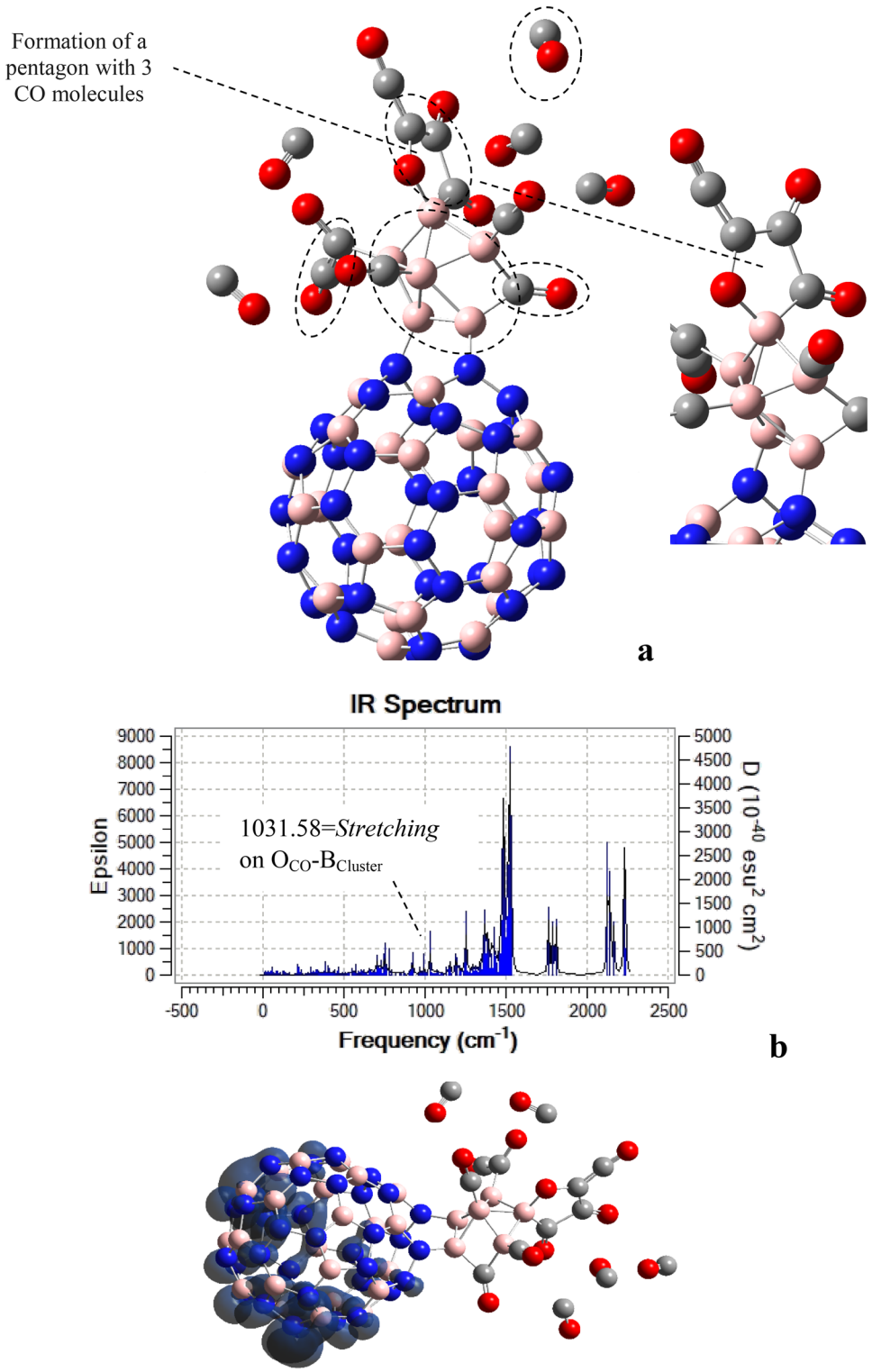

Fig. 12 **a** BNF:B_6–$(CO)_{14}$ molecules for $Q=-1$ and $M=2$, **b** IR spectrum and total spin density surface localized on BN fullerene

4 Conclusions

We have presented studies about retention of carbon monoxide molecules on pristine [BN fullerene]$^-$, [BNF:B_6]$^-$ and [BNF:C_6]$^-$ nanocomposites by means DFT calculations. As result, it was found high chemisorption in all these cases, and the point of saturation was obtained when 14 CO molecules were interacting with the whole pristine cases considered in this work. On the other hand, the global quantum descriptors such as: polarity, the average chemical reactivity and work

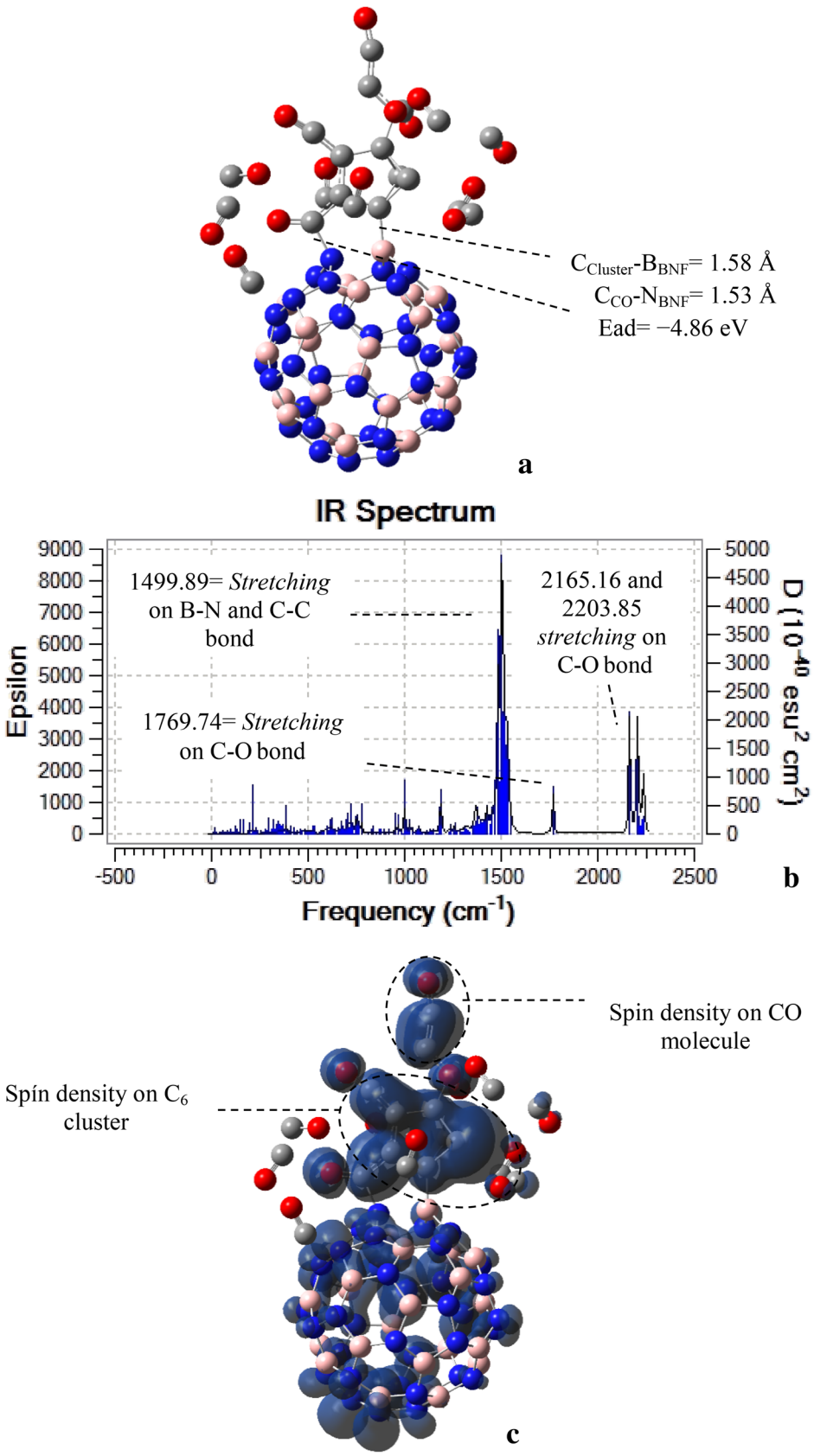

Fig. 13 **a** BNF:C_6–$(CO)_{14}$ molecules for $Q=-1$ and $M=4$, **b** IR spectrum and total spin density surface localized on CO molecule, C_6 cluster and BN fullerene

function were obtained as low values, which indicate the feasibility experimental synthesis. The magnetic moment remains invariant under adsorption of carbon monoxide molecules, except for BNF:C_6–$(CO)_{14}$ case. These nanocomposites show high retention capacity of CO molecules, so they could be a good option to solve this environmental problem.

Acknowledgements This work was partially supported by projects: VIEP-BUAP (CHAE-ING18-G) and Cuerpo Académico Ingeniería en Materiales (BUAP-CA-177). We thank the support given by the National Laboratory Supercomputing Southeast housed in the BUAP.

References

1. C.R. Hoover, Ind. Eng. Chem. **13**(9), 770–772 (1921)
2. F. Cook, Ind. Eng. Chem. Anal. Ed. **12**(11), 661–662 (1940)
3. D.H. Stedman, Environ. Sci. Technol. **23**(2), 147–149 (1989)
4. S.F Liu, S. Lin, T.M. Swager, ACS Sens. **1**(4), 354–357 (2016)
5. L.B. da Silva, S.B. Fagan, R. Mota, Nano Lett. **4**(1), 65–67 (2004)
6. P.K. Dutta, A. Ginwalla, B. Hogg, B.R. Patton, B. Chwieroth, Z. Liang, P. Gouma, M. Mills, S. Akbar, J. Phys. Chem. B **103**(21), 4412–4422 (1999)
7. S.S. Sung, R. Hoffmann, J. Am. Chem. Soc. **107**(3), 578–584 (1985)
8. N. Dimakis, N.E. Navarro, T. Mion, E.S. Smotkin, J. Phys. Chem. C **118**(22), 11711–11722 (2014)
9. J. De Haeck, N. Veldeman, P. Claes, E. Janssens, M. Andersson, P. Lievens, J. Phys. Chem. A **115**(11), 2103–2109 (2011)
10. W.C. McKee, M.C. Patterson, D. Huang, J.R. Frick, R.L. Kurtz, P.T. Sprunger, L. Liu, Y. Xu, J. Phys. Chem. C **120**(20), 10909–10918 (2016)
11. S. Bates, J. Dwyer, J. Phys. Chem. **97**(22), 5897–5900 (1993)
12. K. Gotterbarm, C. Bronnbauer, U. Bauer, C. Papp, H.-P. Steinrück, J. Phys. Chem. C **118**(43), 25097–25103 (2014)
13. A.A. Peyghan, A. Soltani, A.A. Pahlevani, Y. Kanani, S. Khajeh, Appl. Surf. Sci. **270**, 25–32 (2013)
14. S. Sinthika, E.M. Kumar, R. Thapa, J. Mater. Chem. A **2**, 12812–12820 (2014)
15. E. Chigo-Anota, M. Salazar Villanueva, S. Valdez, M. Castro, Struct. Chem. **28**, 1757–1764 (2017)
16. E. Chigo Anota, G. Cárdenas-Jirón, M. Salazar Villanueva, A. Bautista Hernández, M. Castro, Phys. E **94**, 196–203 (2017)
17. E. Chigo Anota, D. Cortés Arriagada, A. Bautista Hernández, M. Castro, Appl. Surf. Sci. **400**, 283–292 (2017)
18. T. Tsuneda, *Density Functional Theory in Quantum Chemistry*. (Springer: Japan, Tokyo, 2014)
19. J. Heyd, G. Scuseria, J. Chem. Phys. **121**, 1187–1192 (2004)
20. R. Ditchfield, W.J. Hehre, J.A. Pople, J. Chem. Phys. **54**, 724–728 (1971)
21. Gaussian 09, Revision D.01, M.J. Frisch, G.W. Trucks, H.B. Schlegel, G.E. Scuseria, M.A. Robb, J.R. Cheeseman, G. Scalmani, V. Barone, B. Mennucci, G.A. Petersson, H. Nakatsuji, M. Caricato, X. Li, H.P. Hratchian, A.F. Izmaylov, J. Bloino, G. Zheng, J.L. Sonnenberg, M. Hada, M. Ehara, K. Toyota, R. Fukuda, J. Hasegawa, M. Ishida, T. Nakajima, Y. Honda, O. Kitao, H. Nakai, T. Vreven, J.A. Montgomery Jr., J.E. Peralta, F. Ogliaro, M. Bearpark, J.J. Heyd, E. Brothers, K.N. Kudin, V.N. Staroverov, T. Keith, R. Kobayashi, J. Normand, K. Raghavachari, A. Rendell, J.C. Burant, S.S. Iyengar, J. Tomasi, M. Cossi, N. Rega, J.M. Millam, M. Klene, J.E. Knox, J.B. Cross, V. Bakken, C. Adamo, J. Jaramillo, R. Gomperts, R.E. Stratmann, O. Yazyev, A.J. Austin, R. Cammi, C. Pomelli, J.W. Ochterski, R.L. Martin, K. Morokuma, V.G. Zakrzewski, G.A. Voth, P. Salvador, J.J. Dannenberg, S. Dapprich, A.D. Daniels, O. Farkas, J.B. Foresman, J.V. Ortiz, J. Cioslowski, D.J. Fox, (Gaussian, Inc., Wallingford, 2013)
22. J. Cano Ordaz, E. Chigo Anota, M. Salazar Villanueva, M. Castro, New J. Chem. **41**, 8045–8052 (2017)
23. P. Geerlings, F. De Proft, W. Langenaeker, Chem. Rev. **103**, 1793–1874 (2003)
24. M. Galvan, A. Vela, J.L. Gázquez, J. Phys. Chem. **92**, 6470–6474 (1988)
25. H. Lu, Z. Liu, X. Yan, D. Li, L. Parent, H. Tian, Sci. Rep. **6**, 24366(1)–(11) (2016)
26. P. Bergveld, J. Hendrikse, W. Olthuis, Meas. Sci. Technol. **9**, 1801–1808 (1998)
27. S. Sinthika, E. Mathan Kumar, V.J. Surya, Y. Kawazoe, N. Park, K. Iyakutti, R. Thapa, Sci. Rep. **5**, 17460(1)–(13) (2015)
28. Q. Sun, Q. J. Am. Chem. Soc. **135**, 8246–8253 (2013)
29. A.S Rad, V.P. Foukolaein, Synth. Met. **210**, 171–178 (2015)
30. A. Shokuhi Rad, D. Sadeghi Shabestary, S.A. Jafari, M. Reza Zardoost, A. Mirabi, Molecular Phys. **114**, 1756–1762 (2016)
31. F. Weinhold, C.R. Landis, *Discovering Chemistry with Natural Bond Orbitals*. (Wiley, Hoboken, 2012)
32. X. Li, X. Wang, J. Zhang, N. Hanagata, X. Wang, Q. Weng, A. Ito, Y. Bando, D. Golberg, Nat. Commun. **8**, 13936(1)–(12) (2017)
33. W. Han, Z. Ma, S. Liu, C. Ge, L. Wang, X. Zhang, Ceram. Int. **43**, 10192–10200 (2017)s